Revista Mexicana de Astronomía y Astrofísica, **44**, 301–309 (2008)

KINEMATICS OF THE NEBULAR COMPLEX MH9/10/11 ASSOCIATED WITH HOIX X-1

P. Abolmasov and A. V. Moiseev

Special Astrophysical Observatory RAS, Russia

Received 2008 April 18; accepted 2008 June 26

RESUMEN

Reportamos los resultados de nuestras observaciones del complejo nebular MH9/10/11 asociado a la ULX HoIX X-1 usando un interferómetro Fabry-Pérot de barrido. Se distinguen dos regiones con distinta cinemática y distintos cocientes de intensidades de líneas, que corresponden aproximadamente a la nebulosa de burbuja MH9/10 y a una región HII más débil, MH11. Para MH9/10 encontramos una tasa de expansión de 20 a 70 km s^{-1}, distinta para la región que se acerca y para la que se aleja. MH11 se caracteriza por una dispersión de velocidades muy pequeña ($\lesssim$ 15 km s^{-1}), y por velocidades a lo largo de la visual casi constantes. Las propiedades de MH11 pueden explicarse mediante la fotoionización de un gas con densidad de hidrógeno de ~ 0.2 cm^{-3}. La luminosidad requerida para ello debe ser del orden de 10^{39} erg s^{-1}. Una fuente igualmente luminosa se requiere también para explicar la expansión de MH9/10. Los resultados del modelo indican también que la abundancia de oxígeno en MH11 es solar.

ABSTRACT

We report the results of our observations of the nebular complex MH9/10/11, associated with the ULX HoIX X-1, with a scanning Fabry-Pérot Interferometer. Two regions differing by their kinematics and line ratios may be distinguished, roughly corresponding to the bubble nebula MH9/10 and the fainter HII-region MH11. For MH9/10 we find an expansion rate of 20 to 70 km s^{-1}that is different for the approaching and receding parts. MH11 is characterised by a very low velocity dispersion ($\lesssim$ 15 km s^{-1}) and nearly constant line-of-sight velocities. The properties of MH11 may be explained by photoionization of a gas with hydrogen density of ~ 0.2 cm^{-3}. The luminosity required for that should be of the order of 10^{39} erg s^{-1}. A source of similar power is required to explain the expansion rate of MH9/10. Modelling results also indicate that the oxygen abundance in MH11 is about solar.

Key Words: ISM: bubbles — ISM: individual (MH9/10/11) — ISM: kinematics and dynamics — X-rays: individual (HoIX X-1)

1. INTRODUCTION

The nature of the Ultraluminous X-ray sources, or ULXs, is first addressed in the work of Fabbiano (1989). These objects were a subject of intense study for the past 20 years and remain one of the unresolved problems in astrophysics (Roberts 2007). Optical observations show that many of these sources are surrounded by large-scale (from tens to hundreds of parsecs) nebulae. We review the properties of some ULX Nebulae (ULXNe) contained in Abolmasov et al. (2007a).

Recent work on ULX environment (Abolmasov et al. 2007b; Ramsey et al. 2006) show that many of these objects are associated with the young (several million years) stellar population, supporting the hypothesis that ULXs are a certain class of accreting binaries with high-mass donor stars. Young SNRs and X-ray bright SNe are excluded from ULXs by definition, though their properties in X-rays may be similar; see discussion in Fabbiano (1989) and references therein. Very often ULXs are found in merging and starburst galaxies.

HoIX is a post-starburst tidal dwarf galaxy lacking old stellar population. We adopt here a distance of 3.6 Mpc as measured by Makarova et al. (2003). According to De Vaucouleurs et al. (1992), line-of-sight velocities of the galaxy are equal to 46 ± 6 km s^{-1} for neutral hydrogen (HI 21 cm) and 119 ± 60 km s^{-1} for the stellar component.

Miller & Hodge (1994) present a survey of all the bright HII-regions —including HoIX— in the M81 group dwarf galaxies in a narrow-band filter sensitive to Hα and [N II]λ 6583. The three brightest HII-regions detected in HoIX form a single extended structure: a bright shell (numbers 9 and 10, according to Miller & Hodge 1994) with some fainter nebulosity (MH11) to the southeast. The spatial dimensions of MH9/10 are 300 pc $\times$ 400 pc. Subsequent work by Miller (1995) identifies the bubble with M81 X-9, or HoIX X-1, which is one of the oldest known ULXs (Fabbiano 1989). The coordinates of the X-ray source as measured by Chandra are $\alpha = 09^h57^m53\overset{s}{.}25$, $\delta = +69°03'48\overset{''}{.}3$ (J2000). With an accuracy of about $0\overset{''}{.}5$ the X-ray source coincides with a relatively bright star with $V \sim 23^{\rm m}$ (Ramsey et al. 2006).

The X-ray source and its environment were extensively studied during the last two decades. It was shown that optical emission lines in the spectrum of MH9/10 are broadened (Ramsey et al. 2006) suggesting that the nebula is powered by shock waves. Optical spectra were acquired with low spectral resolution (Miller 1995; Abolmasov et al. 2007a) revealing some new features, such as He IIλ 4686 emission from the vicinity of the X-ray source. *HST* observations (Ramsey et al. 2006) showed that the X-ray source coincides with a young stellar association. Isochrone fitting points to an age in the range $4-6$ Myr. Ramsey et al. (2006) detected 5 stars in the mass range $12-20\ M_\odot$ implying that the total mass of the association is of the order of $10^3\ M_\odot$. The authors argue that supernova explosions and stellar winds are insufficient to explain the observed luminosity and the size of the bubble.

Pakull & Grisé (2008) report that in the high-ionization [O III]λ 5007 emission line MH11 is about as bright as MH9/10. This points to somewhat different physical conditions in MH11 that may be a consequence of different ionization and heating mechanisms.

Our kinematical study is aimed to acquire more information about both the shell and the high-ionization part of the nebular complex. In the next section we describe our observations with a scanning Fabry-Pérot Interferometer. The main results are given in § 3. We analyse the results for MH9/10 in § 4 and for MH11 in §§ 5 and 6, the latter devoted to photoionization modelling. The results are discussed in § 7.

2. OBSERVATIONS

Our observations were carried out on January 15/16, 2008 at the prime focus of the Russian Special Astrophysical Observatory 6 m telescope with the SCORPIO multi-mode focal reducer (Afanasiev & Moiseev, 2005). We used a scanning Fabry-Pérot Interferometer (FPI) providing a spectral resolution $30-35$ km s^{-1}. The object was observed in two emission lines: [S II]λ 6717 (total exposure 160 s $\times$ 36 spectral channels) and [O III]λ 5007 (total exposure 180 s $\times$ 36 spectral channels). The free spectral range was 13.7 and 7.7 Å, correspondingly. Seeing was around $2-2.5''$ during the observations. The detector was an EEV 42-40 2048×2048 CCD operated with 4×4 binning to reduce the readout time. The spatial scale was $0\overset{''}{.}7$ per pixel.

Reduction was performed in IDL environment using `ifpwid` software designed by one of us (A.V.M.). Data reduction algorithms are described by Moiseev (2002) and Moiseev & Egorov (2008). Line profile parameters were determined by fitting with Voigt functions of fixed Lorentzian widths (30 km s^{-1} for [O III]λ 5007 and 34 km s^{-1} for [S II]λ 6717). The instrumental profile was measured using the spectra of a He-Ne-Ar calibration lamp. The Voigt fitting procedure allows to measure line widths even when they are less than the instrumental profile width (Moiseev & Egorov 2008). Profiles were fitted only in pixels where the flux exceeded 18 ADU (corresponding to a $S/N \sim 3$). All the line-of-sight velocities presented here are heliocentric.

3. RESULTS

Line intensity, line-of-sight velocity and velocity dispersion maps are presented in Figure 1. All the maps where smoothed by a 3×3 median filter. It may be seen that the two parts of the nebula have similar size but vastly different kinematics and line ratios. The velocity dispersion is $\lesssim 15$ km s^{-1} for MH11, but generally exceeds 30 km s^{-1} for MH9/10. MH11 is definitely seen in the [O III] line but not in [S II]λ 6717. As we will see below, the [O III]λ 5007/Hβ flux ratio differs by a factor of ~ 10 for the two nebulae. The [O III]λ 5007 flux from MH11 is 0.65 ± 0.1 that of MH9/10 (the uncertainty is due to the uncertain boundary between the two regions).

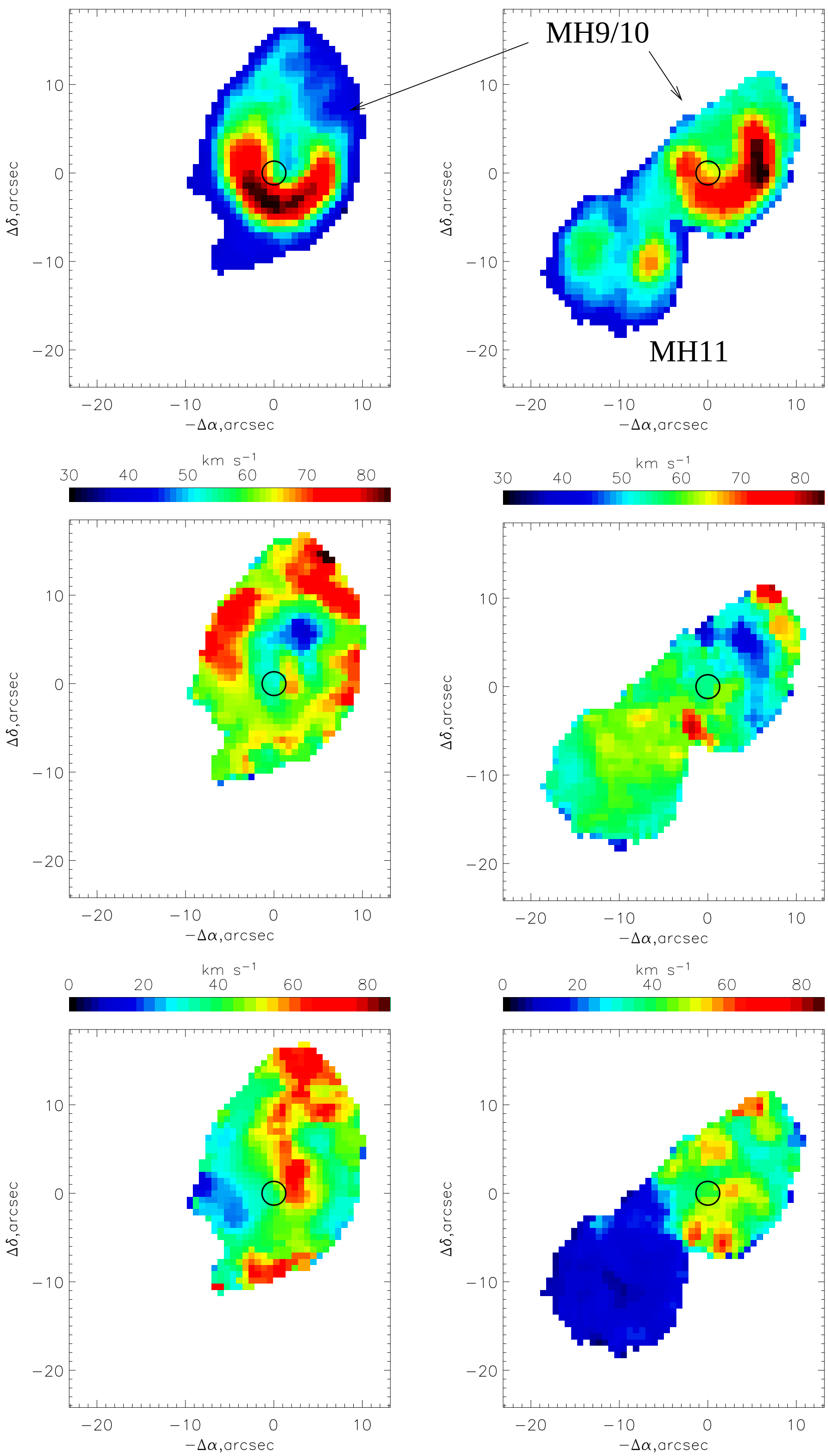

Fig. 1. From top to bottom: intensity, velocity and velocity dispersion maps in the two emission lines, left: [S II]λ 6717; right: [O III]λ 5007. Velocity and velocity dispersion scales are given above the corresponding pictures. The X-ray source is shown by a $1''$ radius circle; the coordinates are given relative to the ULX.

TABLE 1

LINE VELOCITIES AND VELOCITY DISPERSIONS IN DIFFERENT PARTS OF THE NEBULAR COMPLEX

Line	Region	V_r, km s^{-1}	σ_V, km s^{-1}
[O III]λ 5007	MH9/10 (center)	50±2	46±2
	MH9/10E	54±2	36±2
	MH9/10W	45±1	36±1
	MH9/10S	56±1	45±2
	MH11	59±1	12±1
[S II]λ 6717	MH9/10 (center)	37±3	100
		131±8	100
	MH9/10E	62±1	34±1
	MH9/10W	59±1	37±1
	MH9/10S	58±1	40±1
	MH11	60±1	24±1

E, W and S correspond to three spatially distinct regions at the bubble periphery (see text). The [S II] line profile in the central region is fitted with two Gaussian components with velocity dispersion pegged at 100 km s^{-1}.

Information about line profiles from different parts of the nebular complex is summarized in Table 1. Generally, fitting with Voigt profiles was used with appropriate Lorentzian widths. We select several regions of interest shown by black (central) and white (offset regions) rectangles in Figure 2. In order to measure the expansion rate of the nebula we select a rectangular region (30 pixels, $2'' \times 7''$) near the center of the bubble where the expansion should result in mostly line-of-sight motions. The [S II] line profile in the central region is asymmetric, and we fit it with a double Gaussian. Parameters of both components are given in Table 1. The intensities of the two components are 0.28 ± 0.05 and 0.72 ± 0.05 of the total line intensity.

Line profiles are extracted also from three offset regions of the same size located to the West, to the East and to the South from the X-ray source (shown by white dotted lines is Figure 2 and denoted as W, E and S in Table 1).

We also integrate line profiles over the pixels with low velocity dispersion ($D \leq 20$ km s^{-1}) in [O III]λ 5007 that belong mostly to MH11. Hereafter we refer to them as the profiles extracted from MH11. Some pixels at the outer rim of MH9/10 have very narrow unshifted [O III] line profiles (see the [O III] line dispersion map in Figure 1); therefore we suggest that the nature of the emitting gas is the same as that in MH11. In Figure 2 the profiles of both lines extracted from the central region are presented, together with the profile of [O III]λ 5007 from MH11. The mean line-of sight velocity of MH11 is $V_{\rm MH11} = 58 \pm 2$ km s^{-1}, close to the line-of-sight velocities of both the neutral gas and the stellar component of HoIX. Within the uncertainties, is also identical to the line-of-sight velocities of the offset regions in the [S II] line.

We did not make any flux calibrations. However, we used line luminosities for MH9/10 from Abolmasov et al. (2007a) corrected for Galactic absorption. Total line luminosities for MH11 are derived using MH9/10 as calibrator. The luminosities and sizes of the two parts of the nebula are given in Table 2 together with *Cloudy* modelling results (see § 6). Line luminosities for MH9/10 in Table 2 are given according to Miller & Hodge (1994) and Abolmasov et al. (2007a) with flux corrections for the Galactic extinction of $A_V = 0^{\rm m}.26$. Line luminosities for MH11 are estimated using fluxes measured from the two nebulae in our FPI data. The [S II] flux is estimated by integrating the spatial elements where the [O III] emission is detected, and its velocity dispersion is ≤ 20 km s^{-1}.

4. MH9/10

The kinematical properties of the nebula (such as the asymmetric [S II]λ 6717 profile in the central region and the velocity shift between the central and peripheral parts) may be explained by its asymmetric expansion. The [S II] velocity of the peripheral

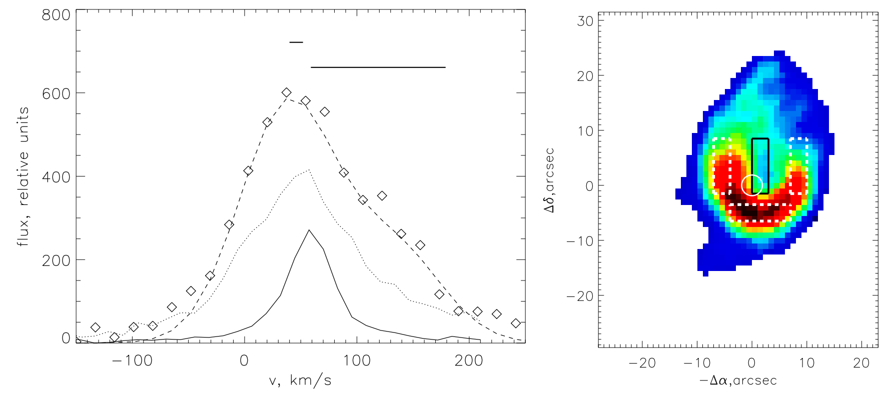

Fig. 2. Left: profiles of [O III]λ5007 integrated over the pixels with low velocity dispersion (solid line, downscaled by a factor of 10) and over the central area of the bubble (dotted). The [S II]λ 6717 line profile from the same central region is shown by diamonds, the dashed curve represents the two-Gaussian fit. Horizontal bars correspond to velocity estimates for stars (lower bar) and HI (upper bar). Right: rectangular region (solid line) defined as the central part of the bubble. Three offset regions are shown by white dotted lines.

regions is consistent with the velocity of the dynamically quiet gas in MH11; hence we consider the systemic velocity equal to 60 km s^{-1}. A two-Gaussian fit of the [S II]λ 6717 line profile shows two velocity components. The line-of-sight velocities of the components are 37 ± 1 km s^{-1} and 131 ± 3 km s^{-1}. The velocity shifts with respect to the systemic velocity of the bubble are -23 and 71 km s^{-1}, respectively, implying that the expansion is anisotropic. The approaching part of the shell is about two times brighter, and its velocity is more than three times closer to the systemic velocity.

The total power of the shock wave may be estimated using expressions from Dopita & Sutherland (1996). Assuming the shell spherical and integrating expression (3.3) from Dopita & Sutherland (1996) over a spherical shock front expanding with constant velocity one obtains:

$$L_{\rm tot} = 7 \times 10^{39}\ R_{150}^2\ V_{50}^3\ n_{10}\ {\rm erg\ s^{-1}}\ , \qquad (1)$$

where n_{10}, R_{150} and V_{50} are correspondingly the preshock hydrogen density (in 10 cm^{-3} units), the shell radius in 150 pc units and the shock velocity in 50 km s^{-1} units. The formula is expected to be valid for radiative, $20-100$ km s^{-1} interstellar shocks, and does not account for precursor emission. A 50 km s^{-1} value is taken as the arithmetic mean of the measured expansion velocities. If one assumes a constant energy influx responsible for powering the nebula, a power of about $10^{39}-10^{40}$ erg s^{-1} is needed (depending on the ambient gas density), similar to the apparent luminosity of the X-ray source.

The Balmer line luminosities are consistent with the expansion velocity estimates made above, if the mean density of the unshocked material is about 5 cm^{-3}. The observed Hβ luminosity of MH9/10 is $(2.73\pm0.13)\times10^{37}$ erg s^{-1} (or higher if additional extinction is present). This value may be compared to the Hβ luminosity calculated using expression (3.4) provided by Dopita & Sutherland (1996):

$$L(H\beta) = 3.8 \times 10^{37}\ V_{50}^{2.41}\ R_{150}^2\ n_{10}\ {\rm erg\ s^{-1}}. \qquad (2)$$

A mean pre-shock density of about $5\ -10$ cm^{-3} is needed to explain the luminosity in Hβ. Multiple shock fronts and anisotropic expansion velocity may be responsible for this rather high effective pre-shock density value. The emergent emission line flux from a unit shock front surface area scales as $F \propto V^{2.41} n$ with the shock velocity and preshock density. Applying this scaling to the flux from the central region points to a ~ 20 times higher pre-shock density for the approaching section of the bubble.

In Figure 2 it may be seen that the [O III] line has a narrow unshifted component present even in the central parts of the bubble. Since 50 km s^{-1} shock waves are incapable of creating precursors we conclude that the unshifted component is emitted either by the warm gas inside the bubble or by a photoionized region similar to MH11 on the line of sight to the bubble.

5. MH11

We confirm the early results of Pakull & Grisé (2008) that the [O III]λ 5007 emission is extremely bright in MH11. From the MPFS observations reported in Abolmasov et al. (2007a) we know the total luminosity (corrected for Galactic absorption only) of the shell in the [O III] line, $L([\rm O\,III]\lambda\ 5007) =$

TABLE 2

LINE LUMINOSITIES AND APPROXIMATE SIZES OF THE TWO PARTS OF THE NEBULAR COMPLEX

Nebula	Line luminosities, 10^{37} erg s^{-1}				R, pc
	Hβ	Hα+[N II]λ 6583	[O III]λ 5007	[S II]λ 6717	
MH9/10	2.73±0.13	11.8±0.5	3.97±0.12	4.3±0.14	150±50
MH11	∼0.27	1.12±0.05	2.6±0.4	0.2±0.02	200±50
Cloudy ($Z = Z_\odot$)	0.26	1.6	2.4	0.4	180
Cloudy ($Z = 0.2Z_\odot$)	0.84	3.0	4.0	0.3	250

In the last column spatial sizes (radius for MH9/10, diameter for MH11) are given. Uncertainties in the radii reflect deviations from circularity. The last two rows correspond to the *Cloudy* model nebulae.

$(3.97\pm0.12)\times10^{37}$ erg s^{-1}. The luminosity of MH11 in the same line is therefore 2.6×10^{37} erg s^{-1}. Because the Hα+[N II]λ 6583 luminosities of MH11 and MH9/10 differ by a factor of 10 (Miller & Hodge 1994), the Hβ luminosity of MH11 should be close to 2.7×10^{36} erg s^{-1}. The [O III]λ 5007/Hβ flux ratio is ~ 10 or higher (if the [N II]λ 6583/Hα ratio is enhanced in the high-excitation nebula). All the line luminosity estimates are given in Table 2.

Quiet kinematics and high [O III]λ5007/Hβ flux ratio favour photoionization as the main energy source in MH11. The Balmer lines are likely to be recombination lines. The Hβ luminosity is determined by the number of ionizing quanta while the [O III] doublet is collisionally excited and is enhanced effectively by additional heating. X-ray and harder EUV radiation may be the additional energy source. The low recombination line luminosity of a large nebula may be a consequence of the low recombining gas density. Let us consider MH11 as a sphere of radius $R = 100$ pc. Assuming the gas completely homogeneous one may estimate the hydrogen density as:

$$n_H \simeq \left(\frac{L(H\beta)}{E(H\beta)\alpha_{\rm eff}(H\beta)V}\right)^{1/2}, \qquad (3)$$

where $V = 4\pi/3R^3$ is the volume of the nebula and $\alpha_{\rm eff}(H\beta) \sim (1-2)\times10^{-14}$cm^3 s^{-1} is the effective recombination coefficient for Hβ at $(1-3)\times10^4$ K in the low-density limit (Osterbrock & Ferland 2006). $E(H\beta)$ is the energy of an Hβ photon. Finally one may estimate the mean hydrogen density in MH11 as:

$$n_H \simeq 0.22\left(\frac{L(H\beta)}{2.7\times10^{36}\ \mathrm{erg\ s^{-1}}}\right)^{1/2}\left(\frac{R}{100\ \mathrm{pc}}\right)^{-3/2}. \qquad (4)$$

6. PHOTOIONIZATION MODELLING

In order to better understand the physics of MH11 and to estimate the parameters of the ionizing source we calculated two *Cloudy* (Ferland et al. 1998) photoionization models. Version 07.02.00 of the code was used. We considered the nebula to be a spherical sector with a covering factor of 0.3 in order to reproduce the offset position of the nebula with respect to the X-ray source. Open geometry was considered (using closed geometry alters the output parameters by $10-15\%$). The gas was irradiated by an EUV blackbody source with variable temperature and luminosity. We used the `optimize` command to find the optimal solution predicting the [O III]λ 5007/Hβ flux ratio and Hβ luminosity closest to the observed values. The hydrogen density was taken equal to 0.2 cm^{-3}. Two abundance sets were used, solar (`HII region` abundance set) and 1/5 solar (`HII region` abundance set with all the heavy-element abundances reduced by a factor of 5).

The best-fit parameters are $T_{\rm BB} = 3\times10^5$ K and $L = 1.9\times10^{39}$ erg s^{-1} for the solar-metallicity model, and $T_{\rm BB} = 1.2\times10^5$ K and $L = 3\times10^{39}$ erg s^{-1} for the subsolar metallicity model. Actually only 30% of these luminosities is used in the calculations because of the covering factor. In Table 2 we present the line luminosities and sizes obtained for the best-fit models. Radii are calculated as the radii of the regions emitting [O III]λ 5007. In lower ionization lines such as [S II]λ 6717 the nebula is expected to be about two times larger; therefore we may underestimate the actual luminosity in the [S II] line. Line emissivities for the two models are shown in Figure 3. Note that the source is located outside the nebula and the observed diameter of the nebula should be compared with the model radii.

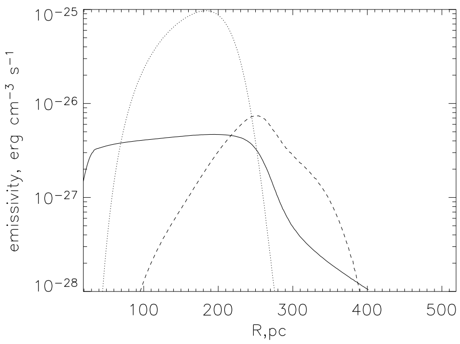

Fig. 3. *Cloudy* model line emissivities as functions of the radial coordinate. Left panel shows the results for solar, right panel for 0.2 solar metallicity. Solid, dashed and dotted lines correspond to Hβ, [S II]λ 6717 and [O III]λ 5007, respectively.

The best-fit solar-metallicity model predicts $L(H\beta) \simeq 3 \times 10^{36}$ erg s^{-1} and [O III]λ 5007/H$\beta \simeq 9$ in reasonable agreement with the observational data. It also predicts that the size of the model nebula should be close to 200 pc, not taking into account the faint low-excitation nebulosity present at larger radii due to X-ray radiation. The *Cloudy* model also predicts bright [O II]λ 3727 emission (about as bright as the [O III]λ 5007 line) and relatively bright low-excitation lines such as the [S II]λ 6717, 6731 doublet with luminosities comparable to Balmer line luminosities.

The best-fit subsolar metallicity model predicts [O III]λ 5007/H$\beta \simeq 4$ and severely overestimates the Hβ luminosity of the nebula. We conclude that subsolar metallicity models have difficulties in reproducing the observed [O III]λ 5007/Hβ ratio possibly indicating that oxygen abundance is around solar for the nebula, rather than $0.1 - 0.2$ solar as reported by Miller (1995). It is probably even higher because both models overestimate the Hα + [N II]λ 6583 luminosity. Certainly, a more thorough investigation involving a larger number of emissions is needed.

7. DISCUSSION

7.1. *Photoionizing Source*

The existence of ULX nebulae supports the idea that ULXs (or at least some of them) are supercritically accreting binaries similar to SS433 (Katz 1986). That analogy allows two energy sources of comparable power to exist, which may be responsible for powering the nebulae: jet activity (jet power is of the order 10^{39} erg s^{-1} in the case of SS433) and photoionizing radiation from the X-ray source. Both are likely to produce HII-regions elongated in the disc/jet symmetry axis direction.

The observational properties of MH11 are consistent with photoionization and heating by a powerful EUV and X-ray source. A high EUV luminosities (comparable to the apparent isotropic luminosities in X-rays) of ULXs is supported both by theory (Poutanen et al. 2007) and by observations (Abolmasov et al. 2008). Therefore, HII-regions similar to MH11 should be common for ULXs. Indeed, there are sources like M101P98 (Abolmasov et al. 2007a; Kuntz et al. 2005) surrounded by extended HII-regions with high [O III]λ 5007/Hβ ratios as well as bubble nebulae overlapped by diffuse structures seen in [O III]λ 5007/Hβ intensity maps as "ionization cones" (Roberts et al. 2003). It is possible that in many cases high-ionization photoionized nebulae are masked by ULX bubbles that have about an order of magnitude higher luminosities in the Balmer lines.

7.2. *Dynamical Properties of the Bubble*

Ramsey et al. (2006) proved that MH9/10 could not be produced by SNe and stellar winds from the parent association of the ULX. There is also evidence that ULX bubbles are produced by continuous power injection by wind or jet activity rather than by instantaneous powerful explosions (Pakull & Grisé 2008; Abolmasov 2008). If one assumes a continuous source of power that heats the gas inside a wind-blown cavern, the expansion law established by Avedisova (1972) (see also Castor, McCray, & Weaver 1975) for pressure-dominated bubbles may be used:

$$R = 70 n_{10}^{-1/5}\, L_{39}^{1/5}\, t_6^{3/5} \text{ pc}, \quad (5)$$

$$V = 40 n_{10}^{-1/5}\, L_{39}^{1/5}\, t_6^{-2/5} \text{ km s}^{-1}. \quad (6)$$

Here L_{39} is the power of the energy source in 10^{39} erg s^{-1} units, n_{10} is the preshock density in 10 cm^{-3} and t_6 is the bubble age in million years.

These formulae may be used to find the kinematical age and the power of the energy source:

$$t = 7 \times 10^5 \, R_{150} \, V_{50}^{-1} \, yr, \quad (7)$$
$$L = 2.8 \times 10^{39} \, R_{150}^2 \, V_{50}^3 \, n_{10} \text{ erg s}^{-1}. \quad (8)$$

A dynamical age $\sim$ 1 Myr is typical for ULX bubbles (Pakull & Mirioni 2003) but higher values were never found supposing the lifetimes of ULXs are of the order of $\sim$1 Myr.

7.3. *Underlying Density Gradient*

Narrow-band images of MH9/10 with higher spatial resolution reveal fine details at the outer boundary of the bubble (Grisé, Pakull, & Motch 2006) and a faint filamentary nebulosity extending to about twice the mean radius of the shell. The complex structure of the bubble is probably connected with a high ambient density gradient. The mean preshock density was probably one or two orders of magnitude higher than the density of the gas in MH11.

Ambient density gradients often lead to blow-out structures and multiple shock fronts (Mac Low, McCray, & Norman 1989). In this perspective, it is tempting to consider MH11 as a blow-out with an invisible outer boundary. The observed gas was ionized by shock waves and is recombining without any additional energy source. The recombination time for the rarefied warm gas is long enough: $t_{\rm rec} \sim 1/n_e \, \alpha \sim$ 1 Myr. The strongest argument against this hypothesis is the quiet kinematics of MH11. If a shock wave propagates in a non-homogeneous medium its velocity varies roughly as $v \propto n^{-1/2}$ (McKee & Cowie 1975). Disturbed gas behind the shock front should have both a high velocity dispersion due to turbulent motions and also a velocity component in the shock propagation direction.

We see however neither the high velocity dispersion (such as tens km s^{-1} or higher) that should inevitably appear if a fast shock was responsible for ionizing the gas nor any strong line-of-sight velocity gradients. The line centroid shifts smoothly by less than 10 km s^{-1} towards the outer rim of the nebula. This shift may appear if the HII-region is expanding due to internal pressure of the warm ionized gas (Osterbrock & Ferland 2006). The expansion velocity is close to the speed of sound in the ionized gas, that is, of the order of 10 km s^{-1}. In Figure 4 we show the behavior of the line profile parameters along the line crossing the central parts of both nebulae at a positional angle of 131°.

Our observations are the first to show that velocity gradients are not an essential part of the dynamics of ULX nebulae. The peak of the [O III] line changes its line-of-sight velocity by less than 10 km s^{-1} for MH11. That is an important clue indicating that on large scales the momentum injected into the ISM is low. ULX nebulae are likely to be powered by radiation and/or relativistic jets that transport negligible amounts of momentum for a given mechanical luminosity.

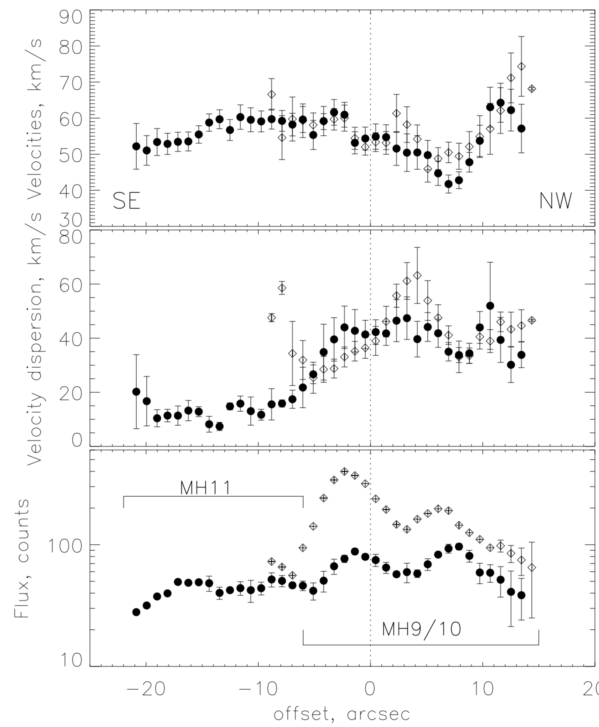

Fig. 4. Cross-section of the line parameter maps by an artificial slit (3.″5 wide) passing through the X-ray source at a position angle 131°. Filled circles represent [O III] line profile parameters and diamonds represent those of the [S II] emission. The offset along the slit is given on the abscissa, zero value corresponding to the X-ray source position.

8. CONCLUSIONS

Observations with a scanning FPI reveal new details about the extended nebular complex associated with HoIX X-1. We measured the expansion rate of MH9/10 and found it consistent with the velocity estimates from Hβ luminosity. However, the expansion appears to be anisotropic. Approaching and receding parts of the bubble have line-of-sight velocities shifted by -23 and 71 km s^{-1} with respect to the systemic velocity of 60 km s^{-1}. The complex structure of the shell probably originates from density gradients that are definitely present in the ISM in HoIX and may be connected to the parent association of the ULX. The dynamical age inferred from the kinematical data is $t \simeq 0.7$ Myr. The mechanical luminosity required is $L \simeq 3 \times 10^{39}$ erg s^{-1}, comparable to the X-ray luminosity of the source. The effective value of the pre-shocked density is $5 - 10$ cm^{-3}.

We show that the observational properties of MH11, namely its high [O III]λ 5007/Hβ ratio (~ 10), size ($\sim$ 200 pc) and Hβ luminosity ($\sim 3 \times 10^{36}$ erg s^{-1}) may be explained by a hard EUV source ionizing low-density gas with $n_H \simeq 0.2$ cm^{-3}. This is the best evidence for an EUV source associated with a ULX available today. A solar oxygen abundance value explains the observational properties of MH11 better than 1/5 solar. The EUV source is well reproduced by a black body with $T \sim (1-2) \times 10^5$ K and isotropic luminosity $L \sim (1-3) \times 10^{39}$ erg s^{-1}. We suggest that further observations are needed in order to decide on the abundances and the ionization balance in MH11.

This work is based on observational data obtained with the 6 m telescope of the Special Astrophysical Observatory of the Russian Academy of Sciences, funded by the Ministry of Science of the Russian Federation (registration number 01-43). We would also like to thank the anonymous referee for his/her very useful remarks and suggestions, and S. Pavluchenko for his help with the English-language.

REFERENCES

Abolmasov, P. 2008, in AIP Conf. Proc., Cool discs, hot flows: The varying faces of accreting compact objects, in press

Abolmasov, P., Fabrika, S., Sholukhova, O., & Afanasiev, V. 2007a, Astrophys. Bull., 62, 36

Abolmasov, P., Fabrika, S., Sholukhova, O., & Kotani, T. 2008, PASJ, submitted

Abolmasov, P., Swartz, D., Fabrika, S., Ghosh, K., Sholukhova, O., & Tennant, A. 2007b, ApJ, 668, 124

Afanasiev, V., & Moiseev, A. 2005, Astron. Lett., 31, 194

Avedisova, V. S. 1972, Soviet Astron., 15, 708

Castor, J., McCray, R., & Weaver, R. 1975, ApJ, 200, L107

De Vaucouleurs, G., de Vaucouleurs, A., Crowin, H, G., Jr., Buta, R. J., Paturel, G., & Fouque, P. 1992, Third Reference Catalogue of bright galaxies (RC3) (`http://vizier.cfa.harvard.edu/viz-bin/VizieR?-source=VII/137B`) (Originally published in New York: Springer-Verlag, 1991)

Dopita, M. A., & Sutherland, R. S. 1996, ApJS, 102, 161

Fabbiano, G. 1989, ARA&A, 27, 87

Ferland, G. J., Korista, K. T., Verner, D. A., Ferguson, J. W., Kingdon, J. B., & Verner, E. M. 1998, PASP, 110, 761

Grisé, F., Pakull, M. W., & Motch, C. 2006, in IAU Symp. 230, Populations of High Energy Sources in Galaxies, ed. E. J. A. Meurs & G. Fabbiano (Cambridge: Cambridge Univ. Press), 302

Katz, J. 1986, Comments Mod. Phys., 11, 201

Kuntz, K. D., Gruendl, R. A., Chu, Y.-H., Chen, C.-H., Still, M., Mukai, K., & Mushotzky, R. 2005, ApJ, 620, 31

Makarova, L. N., et al. 2003, Ap&SS, 285, 107

Mac Low, M. M., MacCray, R., & Norman, M. L. 1989, ApJ, 337, 141

McKee, C. F., & Cowie, L. L. 1975, ApJ, 195, 715

Miller, B. W. 1995, ApJ, 446, 75

Miller, B. W., & Hodge, P. 1994, ApJ, 427, 656

Moiseev, A. V. 2002, Bull. Spec. Astrophys. Obs., 54, 74

Moiseev, A. V., & Egorov, O. V. 2008, Astrophys. Bull., 63, 181

Osterbrock, D. E., & Ferland, G. 2006, Astrophysics of Gaseous Nebulae and Active Galactic Nuclei, ed. D. E. Osterbrock & G. J. Ferland (2nd ed.; Sausalito: Univ. Sci. Books)

Pakull, M. W., & Grisé, F. 2008, in AIP Conf. Proc. 1010, Population Explosion: The Nature and Evolution of X-ray Binaries in Diverse Environments, ed. R. M Bandyopadhyay, S. Wachter, D. Gelino & C. R. Gelino (New York: AIP), 303

Pakull, M. W., & Mirioni, L. 2003, RevMexAA (SC), 15, 197

Poutanen, J., Lipunova, G., Fabrika, S., Butkevich, A., & Abolmasov, P. 2007, MNRAS, 377, 1187

Ramsey, C. J., Williams, R. M., Gruendl, R. A., Chen, C.-H. R., Chu, Y.-H., & Wang, Q. D. 2006, ApJ, 641, 241

Roberts, T. P. 2007, Ap&SS, 311, 203

Roberts, T. P., Goad, M. R., Ward, M. J., & Warwick, R. S. 2003, MNRAS, 342, 709

P. Abolmasov and A. V. Moiseev: Special Astrophysical Observatory, Nizhnij Arkhyz, Zelenchukskij region, Karachai-Cirkassian Republic, Russia 369167 (pasha, moisav@sao.ru).